Effect of B4C addition on mechanical and electrical properties of Ca3Co4O9

Hippolyte Amaveda
Instituto de Ciencias de Materiales de Aragon
Mario Mora
Instituto de Ciencias de Materiales de Aragon
Oscar J Dura
Universidad de Castilla-La Mancha Escuela Tecnica Superior de Ingenieros Industriales
Miguel A Torres
Instituto de Ciencias de Materiales de Aragon
Maria A Madre
Instituto de Ciencias de Materiales de Aragon
Sylvain Marinel
Ecole Nationale Superieure d'Ingenieurs de Caen
A. Sotelo (asotelo@unizar.es)
Instituto de Ciencias de Materiales de Aragon https://orcid.org/0000-0001-7056-0546

Research Article

Keywords: Ceramics, Sintering, Mechanical properties, Thermoelectric, Thermal expansion

Posted Date: April 15th, 2020

DOI: https://doi.org/10.21203/rs.3.rs-22821/v1

Abstract

B4C added Ca3Co4O9 in different proportions (0, 0.1, 0.25, 0.5, and 0.75 wt.%) have been fabricated using solid-state method. Powder XRD patterns have shown that only Ca3Co4O9 phase can be identified in all the samples. Microstructural observations have allowed determining that B4C compound has been superficially oxidized, producing liquid B2O3 phase during sintering, which has reacted with the Ca3Co4O9 grains to produce bridges between them. In spite of the increase of porosity, these bridges led to an important raise (more than two times) of mechanical properties. On the other hand, while B4C addition has not significantly influenced S values, it has decreased electrical resistivity, thermal conductivity, and thermal expansion. Consequently, ZT values have been also increased, reaching 0.24 in 0.25 wt.% B4C containing samples, which is very close to the best values reported in the literature for Ca3Co4O9 compounds, and two times higher than the obtained in pure materials in this work.

Introduction

Thermoelectric (TE) technology is considered as a very promising one to enhance energy transforming devices efficiency by harvesting wasted heat [1]. This characteristic is associated to the Seebeck effect inherent to the TE materials [2]. On the other hand, these materials should have appropriate thermoelectric properties, evaluated using the equation [3]:

$$ZT = \frac{S^2 T \sigma}{\kappa} \quad \text{(Eq. 1)}$$

where *ZT* is the dimensionless Figure-of-Merit, and S, T, σ, and κ are Seebeck coefficient, absolute temperature, electrical, and thermal conductivity, respectively.

TE materials are considered adequate for practical applications when their *ZT* values are higher than 1. Nowadays, only intermetallic materials display these values at low-medium temperatures [4, 5], with the drawback of their usual heavy elements content. Moreover, they cannot be used at high temperatures due to oxidation processes, unless they are encapsulated to avoid oxidant environments. On the other hand, oxide materials possess high chemical and thermal stability, and can work at high temperatures. Moreover, they are composed of abundant, cheaper, and environmentally friendly elements [6]. However, their TE performances are lower than those determined in intermetallic materials. Consequently, most of the works published in this field are dealing with the improvement of their TE performances through many different ways [7–13].

Nevertheless, TE properties of materials are not the only parameters determining the efficiency of a TE module. One of them is the so-called manufacturing factor (MF) which is a function of the ideal resistance in the module (R_{id}, taking into account the resistance of legs), and the real internal resistance (R_{int}, where the contact resistance is also present), as MF = R_{id}/R_{int} [14]. This MF is usually determined in the as-fabricated modules, but it can be decreased during the working life of these modules due to the differential expansion of the different components (*p*, and *n* thermoelectric legs, metallic parts, and

insulating ceramic) which can damage the contacts among them, increasing the internal resistance. Consequently, before building a TE module, it is very convenient to choose materials with very close thermal expansion coefficients to avoid internal stresses when working at high temperature. Besides, high mechanical properties are also desired in these TE legs in order to maintain the module integrity to increase its useful life.

In this work, $Ca_3Co_4O_9$ material will be prepared, with the addition of small amounts of B_4C (0, 0.10, 0.25, 0.50, and 0.75 wt.%) via the classical solid-state route. The effect of these additions on the structure and microstructure of $Ca_3Co_4O_9$ sintered pellets will be studied, and related to the modifications of linear expansion coefficient, mechanical, and thermoelectric properties.

Experimental

$Ca_3Co_4O_9$ + x wt.% B_4C, with x = 0.0, 0.10, 0.25, 0.50, and 0.75, have been prepared using the classical solid-state route from $CaCO_3$ (Panreac, 98 + %), and Co_2O_3 (Aldrich, 98 + %) commercial powders. They were weighed in the adequate amounts, mixed and ball milled under water media for 30 minutes at 300 rpm to produce a suspension, which was dried under infrared radiation. The resulting dry mixture was manually milled to produce a very fine powder, subsequently thermally treated at 750 and 800 ºC for 12 h under air, with an intermediate manual milling. This thermal process is adequate to decompose $CaCO_3$ and to produce intermediate by-products, in agreement with previously reported data [15]. After milling these calcined powders, B_4C (Alfa Aesar, 99 + %) has been added in the stoichiometric proportions and the mixture has been ball milled 30 minutes at 300 rpm to homogenize the mixture. After this process, the different materials were cold-pressed in form of pellets under 400 MPa applied pressure. Finally, the compacts were sintered at 900 ºC for 24 h under air atmosphere, followed by a final furnace cooling.

Powder X-ray diffraction (XRD) patterns were determined in a theta-theta PANalyticalX'Pert Pro diffractometer (CuKα radiation, λ = 1.54059 Å) between 10 and 40 degrees, where the main peaks of $Ca_3Co_4O_9$ phase, and the most intense of B_4C, appear. Density measurements were performed using Archimedes' method on several samples for each B_4C addition. The relative density values were calculated with respect to the theoretical one, assuming a dense and perfect mixture of $Ca_3Co_4O_9$ (4.677 g/cm^3 [16]) and B_4C (2.50 g/cm^3 [17]).

Microstructural observations have been performed on the samples surfaces and fractured sections in a Field Emission Scanning Electron Microscope (FESEM, Carl Zeiss Merlin) combined with an energy-dispersive spectrometry (EDS) system. Flexural strength has been determined in several samples for each composition using the three point bending test in an Instron 5565. Samples were measured with 30 μm/s punch displacement and 10 mm span. Seebeck coefficient and electrical resistivity were simultaneously determined through the four-point contact using a LSR-3 (Linseis GmbH) under He atmosphere in the 50–800 ºC temperature range. Thermal diffusivity (α) has been measured in a laser-flash system (Linseis LFA

1000). Thermal conductivity (κ) has been calculated as $\kappa = a \cdot C_p \cdot \rho$, being C_p specific heat and ρ, sample density. C_p has been determined through Dulong-Petit law. In order to stablish the samples TE performances, ZT was determined from Seebeck coefficient, electrical resistivity, and thermal conductivity data. These data were used to evaluate the properties evolution as a function of the dopant content, and were also compared with previously reported values in the literature for similar compounds. Finally, dilatometric behaviour of samples has been studied in the 25–800 ºC temperature range in a L79 HCS dilatometer (Linseis GmbH) to determine their linear expansion coefficient evolution as a function of B_4C content.

Results And Discussion

Figure 1 illustrates the XRD patterns obtained in $Ca_3Co_4O_9$ + x wt.% B_4C powdered samples. As it can be easily observed in the figure, all samples present the same patterns, independently of the B_4C addition. Moreover, all peaks can be associated to the diffraction planes (indicated in the graph) of $Ca_3Co_4O_9$ phase with monoclinic symmetry [18, 19]. Furthermore, the most intense diffractions correspond to its *ab*-planes, which could be associated to preferential grain orientation. However, it should be highlighted that XRD patterns were obtained on powdered samples and, consequently, this grain orientation is produced by the samples preparation, as observed in previous works [20]. On the other hand, no B_4C has been identified with this technique, probably due to its small amount, and the fact that its most intense peak appears at 39.4 degrees [21], together with a possible partial decomposition during sintering, and it can be masked by the (020) diffraction of $Ca_3Co_4O_9$ phase.

Figure 2 presents several representative SEM micrographs performed on the samples surfaces. These images show that all samples are composed of flake-like particles with no preferential orientation, which is the characteristic situation in this system, as reported in previous works [22, 23]. Moreover, all grains composition has been determined, through EDS, as $Ca_3Co_4O_9$ phase, confirming the XRD results previously presented. On the other hand, the $Ca_3Co_4O_9$ grain sizes are decreased, when the amount of B_4C in the samples is increased, while porosity seems to be increased. In order to confirm the raise in porosity when the B_4C content is larger, the samples density was evaluated and the mean results, together with their standard error, are displayed in Table 1. As it is clear from these data, samples density is slightly decreased when the amount of B_4C is increased, corroborating the SEM observations. In any case, the relative density values are in the order of the typically reported in materials prepared through the classical solid-state method [23–25]. This low densification can be explained when considering the phase equilibria diagram [26], which shows that $Ca_3Co_4O_9$ phase is stable up to 926 ºC. Consequently, sintering procedure has to be performed below this temperature, which is, in turn, much lower than the eutectic temperature (1350 ºC), drastically limiting the samples densification.

Figure 3 presents the three point bending tests results for the $Ca_3Co_4O_9$ and their standard errors, as a function of B_4C content. In spite of the slight decrease of density induced by B_4C addition, mechanical properties are drastically increased, when compared to the pure samples. It is increased in around 50% for

0.1% B_4C addition, and more than 100% for higher contents. These results seem to be contradictory and, consequently, the fractured sections of samples were microstructurally studied. Figure 4 shows a representative micrograph at high magnification of 0.75 B_4C sample. As it can be observed in the picture, besides the grey contrast ($Ca_3Co_4O_9$ phase), a new contrast (dark grey) is appearing. EDS analysis has shown that this contrast contains B, C, O, Ca, and Co, and it is connecting thermoelectric grains. This behaviour can be explained when considering that B_4C starts to be oxidized under air at around 450 ºC, producing CO_2 and B_2O_3 [27]. This effect could lead to the total B_4C oxidation, however, the formed B_2O_3 has melting point of 450 ºC [28] and, between 600 and 1000 ºC, forms a protective layer on the particles surface avoiding further oxidation [29]. On the other hand, the presence of this liquid phase, making close contact with the thermoelectric grains, lead to Ca-B-O [30], and Co-B-O [31] compounds formation on the B_4C particles surface. Consequently, these compounds form bridges between the thermoelectric grains, enhancing the samples mechanical properties.

Electrical resistivity variation with temperature, as a function of B_4C content is presented in Fig. 5. As shown in the plot, all samples possess very similar behaviour in the whole measured temperature range. The samples display a minimum at around 450 ºC, which corresponds to the change between semiconducting ($d\rho/dT < 0$) and metallic ($d\rho/dT > 0$) behaviour. This temperature indicates the change from a hole hopping from Co^{4+} to Co^{3+} [32] to a charge carriers transport in the valence or conduction band [33]. This is a very common behaviour observed in $Ca_3Co_4O_9$ sintered materials [23, 34]. On the other hand, B_4C addition up to 0.25 wt.% decreases electrical resistivity, while further addition drastically increases it, when compared to samples without additions. This behaviour with B_4C is similar to the one observed in thin films, where a slightly lower Co content, with respect to the stoichiometric one, leads to lower electrical resistivity [35]. Moreover, this effect also induces a lower grain size, which agrees with the previous observations. On the other hand, the decrease of electrical resistivity of B_4C containing samples, when compared to the pure ones, is lower than the observed in [35], which can be associated to a lower reduction of Co content. Furthermore, the formation of B-containing phases in these samples can also affect the electrical transport properties. Consequently, the lowest electrical resistivity values have been obtained in samples with 0.25 wt.% B_4C. The minimum resistivity values measured in these samples at 800 ºC (14 mΩ cm) are slightly lower than the best values reported for $Ca_3Co_4O_9$ samples sintered or textured through spark plasma sintering (15–18 mΩ cm) [36] and around 20% lower than in pure samples. However, they are higher than the measured in highly dense materials prepared using alternative methods (10 mΩ cm) [37].

Figure 6 shows the S variation with temperature and B_4C content. In all cases S shows positive values, indicating that conduction is mainly produced by holes. Moreover, the behaviour is the same for all samples, the values are increased when the temperature rises, and these values are the same for all samples within the measurement errors. These very close S values, independently of B_4C content can be explained by the very small compositional modification produced in the samples discussed previously. Furthermore, the cations drainage induced by the liquid B_2O_3 is probably limited to the zones close to the

grain boundaries, maintaining the core of the grains unchanged. Consequently, no significant modifications in S values should be expected. The highest values at 800 ºC (195 μV/K) are higher than the reported in pure $Ca_3Co_4O_9$ sintered or textured through spark plasma sintering (170–175 μV/K) [36], but lower than the reported in very dense materials obtained by alternative methods (205 μV/K) [37].

Total κ consists in the addition of two components, $\kappa = \kappa_l + \kappa_e$, where κ_l is the lattice thermal conductivity contribution and κ_e is the electronic counterpart. κ_e can be estimated from the Wiedemann-Franz's law [38], which is expressed as $\kappa_e = L\ \sigma\ T$, where *L, and* σ are Lorenz number ($2.45 \times 10^{-8}\ V^2/K^2$), and electrical conductivity, respectively. The variation with temperature and B_4C content of the electronic and total thermal conductivity are presented in Fig. 7. When comparing both graphs, it is clear that electronic thermal conductivity is increased when the temperature rises. In contrast, the total thermal conductivity decreases from room temperature to around 600–650 ºC induced by the increase of lattice vibrations which enhance phonon scattering. At higher temperatures, the total thermal conductivity increases due to the larger influence of electronic thermal conductivity. Moreover, B_4C addition leads to a clear decrease of total thermal conductivity, when compared to the pure samples, especially at high temperatures. These results are in agreement with previous works in $Ca_{3-x}B_xCo_4O_9$ which showed that thermal conductivity is decreased with B-content up to 0.5 [39]. At 800 ºC, the minimum total thermal conductivity value determined in 0.25 wt.% B_4C samples (1.2 W/K m) is about 20% higher than the lowest measured in these samples (1.0 W/K m at 650 ºC). Moreover, these values are comparable to the reported in classically sintered materials (0.9 W/K m with ~ 60% theoretical density) which show higher amount of porosity [40] than the samples in this work. On the other hand, it is lower than the best values obtained by spark plasma sintering (2.1 W/K m) [41], and much lower than the measured in textured materials by hot-uniaxial pressing (2.2, 3, and 4.7 W/K m) [13, 40, 42].

With all the previously discussed data, ZT has been calculated and plotted in Fig. 8. As displayed in the graph, ZT values are increased with temperature in the whole measured temperature range, and also with B_4C content up to 0.25 wt.%, decreasing for higher additions. The highest value has been measured at 800 ºC in 0.25 wt.% B_4C samples (0.24), which is more than two times higher than the calculated for pure ones. Moreover, it is higher than the measured in classically (0.08 [40]), or spark plasma sintered samples (0.15 [41]), and even than the determined in textured samples (0.18, and 0.16 [13, 40]). However, this value is lower than the reported one for materials prepared through non-conventional methods (0.35 [15]) or in $Ca_{3-x}Sr_xCo_4O_9$ textured materials (0.29 [42]).

Thermal expansion coefficient has been determined in all samples and presented in Table 2. As it can be observed in this table, thermal expansion of pure samples (10.32 ppm/K) is in the range of the reported value for $Ca_3Co_4O_9$ materials (10.6 ppm/K [25]) and lower than the measured in Bi-substituted materials (12.8 ppm/K [25]). On the other hand, B_4C addition, up to 0.25 wt.%, decreases thermal expansion coefficient, increasing with further additions. The minimum value (9.3 ppm/K) measured in this work corresponds to a decrease of only around 10% but closer to the one reported for Al_2O_3 (7.5 ppm/K [43]). This reduction, even if it does not seem to be significant, may reduce the differential thermal expansion

between two of the main components of thermoelectric modules, decreasing the internal stresses at working temperatures, and increasing the life span of these devices.

Conclusions

$Ca_3Co_4O_9$ + x wt.% B_4C (x = 0, 0.1, 0.25, 0.5, and 0.75) polycrystalline materials have been prepared through the classical ceramic method. XRD analysis has only identified $Ca_3Co_4O_9$ phase in all samples, independently of the B_4C content. SEM observations have shown that B_4C has reacted with oxygen producing liquid B_2O_3 on its surface, slightly reacting with $Ca_3Co_4O_9$ grains and forming bridges between the grains. These microstructural modifications have been reflected in the mechanical properties, which were enhanced when compared with the pure samples, despite the slight increase of porosity. Seebeck coefficient has not been affected by B_4C addition, while electrical resistivity, thermal conductivity and thermal expansion have been decreased, leading to maximum ZT values close to the best reported in the literature, and about two times higher than the measured in pure samples in this work. It is worth to mention that these results have been obtained through a simple and scalable process which can be easily transferred to industry.

Declarations

Acknowledgements

The authors wish to thank the Gobierno de Aragón-FEDER (Research Group T 54-17R), and the Spanish MINECO-FEDER (Project MAT2017-82183-C3-1-R) for financial support. Authors would like to acknowledge the use of Servicio General de Apoyo a la Investigación-SAI, Universidad de Zaragoza.

Data Availability

The raw/processed data required to reproduce this work cannot be shared at this time as they forms part of an ongoing study.

References

1. Mahan G, Sales B, Sharp J. Thermoelectric materials: New approaches to an old problem. Phys Today. 1997;50:42–7.
2. Seebeck TJ. Magnetic polarization of metals and minerals. *Abhandlungen der Deutschen Akademie der Wissenschafren zu Berlin* 1822, **265**: 1822–1823.
3. Rowe DM. Thermoelectrics handbook: macro to nano. Boca Raton: CRC Press; 2006.
4. Wang H, Hwang J, Snedaker ML, et al. High Thermoelectric Performance of a Heterogeneous PbTe Nanocomposite. Chem Mater. 2015;27:944–9.
5. Wang X, Wang HC, Su WB, et al. Geometric structural design for lead tellurium thermoelectric power generation application. Renew Energy. 2019;141:88–95.

6. Yaroshevsky AA. Abundances of chemical elements in the Earth's crust. Geochem Int. 2006;44:48–55.
7. Itahara H, Xia C, Sugiyama J, et al. Fabrication of textured thermoelectric layered cobaltites with various rock salt-type layers by using β-$Co(OH)_2$ platelets as reactive templates. J Mater Chem. 2004;14:61–6.
8. Sotelo A, Rasekh Sh, Torres MA, et al. Effect of synthesis methods on the $Ca_3Co_4O_9$ thermoelectric ceramic performances. J Solid State Chem. 2015;221:247–54.
9. Shi Z, Xu J, Zhu J, et al. Effect of platelet template seeds on microstructure and thermoelectric properties of $Ca_3Co_4O_9$ ceramics. Ceram Int. 2019;45:1977–83.
10. Liu Y, Lin Y, Nan C-W, et al. Preparation of $Ca_3Co_4O_9$ and improvement of its thermoelectric properties by spark plasma sintering. J Am Ceram Soc. 2005;88:1337–40.
11. Delorme F, Diaz-Chao P, Guilmeau E, et al. Thermoelectric properties of $Ca_3Co_4O_9$–Co_3O_4 composites. Ceram Int. 2015;41:10038–43.
12. Schulz T, Topfer J. Thermoelectric properties of $Ca_3Co_4O_9$ ceramics prepared by an alternative pressure-less sintering/annealing method. J Alloys Compds. 2016;659:122–6.
13. Wang H, Sun X, Yan X, et al. Fabrication and thermoelectric properties of highly textured $Ca_9Co_{12}O_{28}$ ceramic. J Alloys Compds. 2014;582:294–8.
14. Lemonnier S, Goupil C, Noudem J. Four-leg $Ca_{0.95}Sm_{0.05}MnO_3$ unileg thermoelectric device. J Appl Phys. 2008;104:014505.
15. Sotelo A, Costa FM, Ferreira NM, et al. Tailoring $Ca_3Co_4O_9$ microstructure and performances using a transient liquid phase sintering additive. J Eur Ceram Soc. 2016;36:1025–32.
16. Liou YC, Tsai WC, Lin WY, et al. Synthesis of $Ca_3Co_4O_9$ and $CuAlO_2$ ceramics of the thermoelectric application using a reaction-sintering process. J Aust Ceram Soc. 2008;44:17–22.
17. Haynes WM, Bruno TJ, Lide DR. CRC Handbook of Chemistry and Physics. Florida: CRC press; 2016.
18. Woermann E, Muan A. Phase equilibria in the system CaO-cobalt oxide in air. J Inorg Nucl Chem. 1970;32:1455–9.
19. JCPDS. 21–0139.
20. Karakaya GC, Ozcelik B, Torres MA, et al. Effect of Na-doping on thermoelectric and magnetic performances of textured $Bi_2Sr_2Co_2O_y$ ceramics. J Eur Ceram Soc. 2018;38:515–20.
21. Dera P, Manghnani MH, Hushur A, et al. New insights into the enigma of boron carbide inverse molecular behavior. J Solid State Chem. 2014;215:85–93.
22. Delorme F, Martin CF, Marudhachalam P, et al. Synthesis of thermoelectric $Ca_3Co_4O_9$ ceramics with high ZT values from a Co^{II} Co^{III}-Layered Double Hydroxide precursor. Mater Res Bull. 2012;47:3287–91.
23. Klyndyuk AI, Matsukevich IV. Synthesis, Structure, and Properties of $Ca_3Co_{3.85}M_{0.15}O_{9+\delta}$ (M = Ti–Zn, Mo, W, Pb, Bi) Layered Thermoelectrics. Inorg Mater. 2015;51:944–50.

24. Shi Z, Gao F, Xu J, et al. Two–step processing of thermoelectric $(Ca_{0.9}Ag_{0.1})_3Co_4O_9$/nano–sized Ag composites with high ZT. J Eur Ceram Soc. 2019;39:3088–93.
25. Matsukevich IV, Klyndyuk AI, Tugova EA, et al. Thermoelectric Properties of $Ca_{3-x}Bi_xCo_4O_{9+\delta}$ ($0.0 \leq x \leq 1.5$) Ceramics. Inorg Mater. 2016;52:593–9.
26. Sedmidubsky D, Jakes V, Jankovsky O, et al. Phase equilibria in Ca–Co–O system. J Solid State Chem. 2012;194:199–205.
27. Litz LM, Mercuri RA. Oxidation of Boron Carbide by Air, Water and Air-Water Mixtures at Elevated Temperatures. J Electrochem Soc. 1963;110:921–5.
28. Cordfunke EHP, Konings RJM. Thermochemical Data for Reactor Materials and Fission Products. North-Holland: Elsevier Science Publishers; 1990.
29. Belovsky L. Heat release from B_4C oxidation in steam and air. *IAEA-TECDOC-921*, International Atomic Energy Agency (IAEA), 1996, 49–61.
30. Yu H, Chen Q, Jin ZP. Thermodynamic assessment of the $CaOB_2O_3$ system. Calphad. 1999;23:101–11.
31. Belyaev IN. K Voprosu o diagramme sostoyaniya sistemy CoO-B_2O_3. Zh Fiz Khim. 1956;30:1419–9.
32. Lin YH, Lan J, Shen ZJ, et al. High-temperature electrical transport behaviors in textured $Ca_3Co_4O_9$-based polycrystalline ceramics. Appl Phys Lett. 2009;94:072107.
33. Pinitsoontorn S, Lerssongkram N, Keawprak N, et al. Thermoelectric properties of transition metals-doped $Ca_3Co_{3.8}M_{0.2}O_{9+\delta}$ (M = Co, Cr, Fe, Ni, Cu and Zn). J Mater Sci Mater Electron. 2012;23:1050–6.
34. Rasekh Sh, Torres MA, Constantinescu G, et al. Effect of Cu by Co substitution on $Ca_3Co_4O_9$ thermoelectric ceramics. J Mater Sci Mater Electron. 2013;24:2309–14.
35. Zhang L, Tan TT, Li S. The effects of composition deviations on the microstructure and thermoelectric performance of $Ca_3Co_4O_9$ thin film. J Mater Sci Mater Electron. 2018;29:13321–7.
36. Kenfaui D, Bonnefont G, Chateigner D, et al. $Ca_3Co_4O_9$ ceramics consolidated by SPS process: Optimisation of mechanical and thermoelectric properties. Mater Res Bull. 2010;45:1240–9.
37. Madre MA, Costa FM, Ferreira NM, et al. Preparation of high-performance $Ca_3Co_4O_9$ thermoelectric ceramics produced by a new two-step method. J Eur Ceram Soc. 2013;33:1747–54.
38. Fine ME, Hsieh N. Wiedermann-Franz-Lorenz relation in highly electronic-conducting oxides. J Am Ceram Soc. 1974;57:502–3.
39. Altin S, Bayri A, Demirel S, et al. Thermal conductivity and magnetic properties of the B substituted $Ca_3Co_4O_9$. Curr Appl Phys. 2014;14:590–5.
40. Kenfaui D, Lenoir B, Chateigner D, et al. Development of multilayer textured $Ca_3Co_4O_9$ materials for thermoelectric generators: Influence of the anisotropy on the transport properties. J Eur Ceram Soc. 2012;32:2405–14.
41. Tian R, Zhang T, Chu D, et al. Enhancement of high temperature thermoelectric performance in Bi, Fe co-doped layered oxide-based material $Ca_3Co_4O_{9+\delta}$. J Alloys Compds. 2014;615:311–5.

42. Torres MA, Costa FM, Flahaut D, et al. Significant enhancement of the thermoelectric performance in $Ca_3Co_4O_9$ thermoelectric materials through combined strontium substitution and hot pressing process. J Eur Ceram Soc. 2019;39:1186–92.
43. Engberg CJ, Zehms EH. Thermal Expansion of Al_2O_3, BeO, MgO, B_4C, SiC, and TiC Above 1000 °C. J Am Ceram Soc. 1959;42:300–5.

Tables

Table 1. Apparent density, standard error, and relative density determined through Archimede's method.

B_4C content (wt.%)	Density (g/cm^3)	Std. error	Relative density
0	3.4532	0.0317	73.8
0.10	3.4358	0.0830	73.6
0.25	3.3742	0.0627	72.3
0.5	3.3205	0.0289	71.3
0.75	3.3009	0.0502	71.0

Table 2. Thermal expansion coefficient (a) determined in $Ca_3Co_4O_9$ + x wt.% B_4C samples.

B_4C content (wt.%)	a (ppm/K)
0	10.32
0.10	9.65
0.25	9.36
0.5	9.56
0.75	9.68

Figures

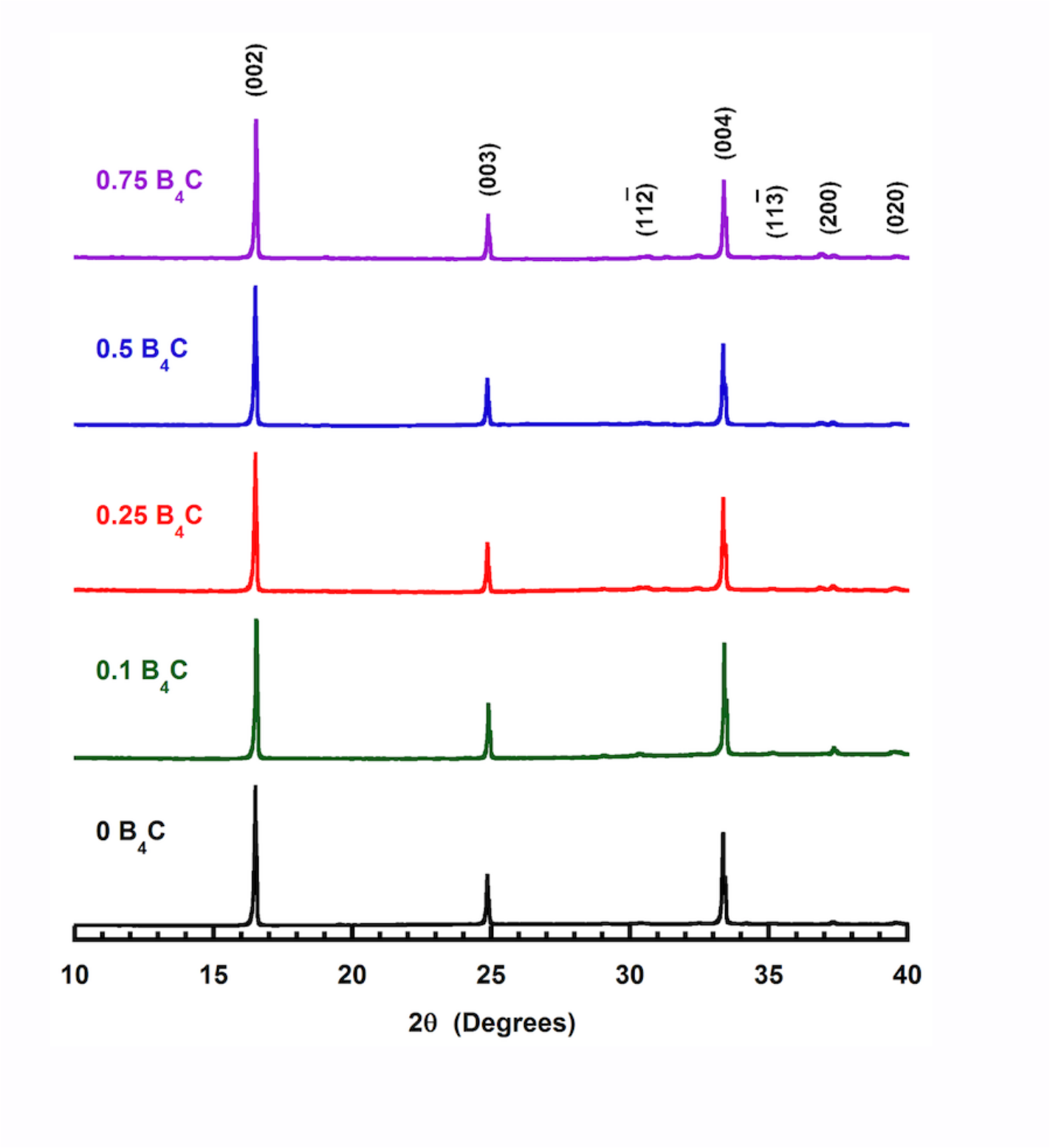

Figure 1

Powder X-ray diffraction patterns of Ca3Co4O9 + x wt.% B4C samples. The diffraction planes indicate the reflections of Ca3Co4O9 phase.

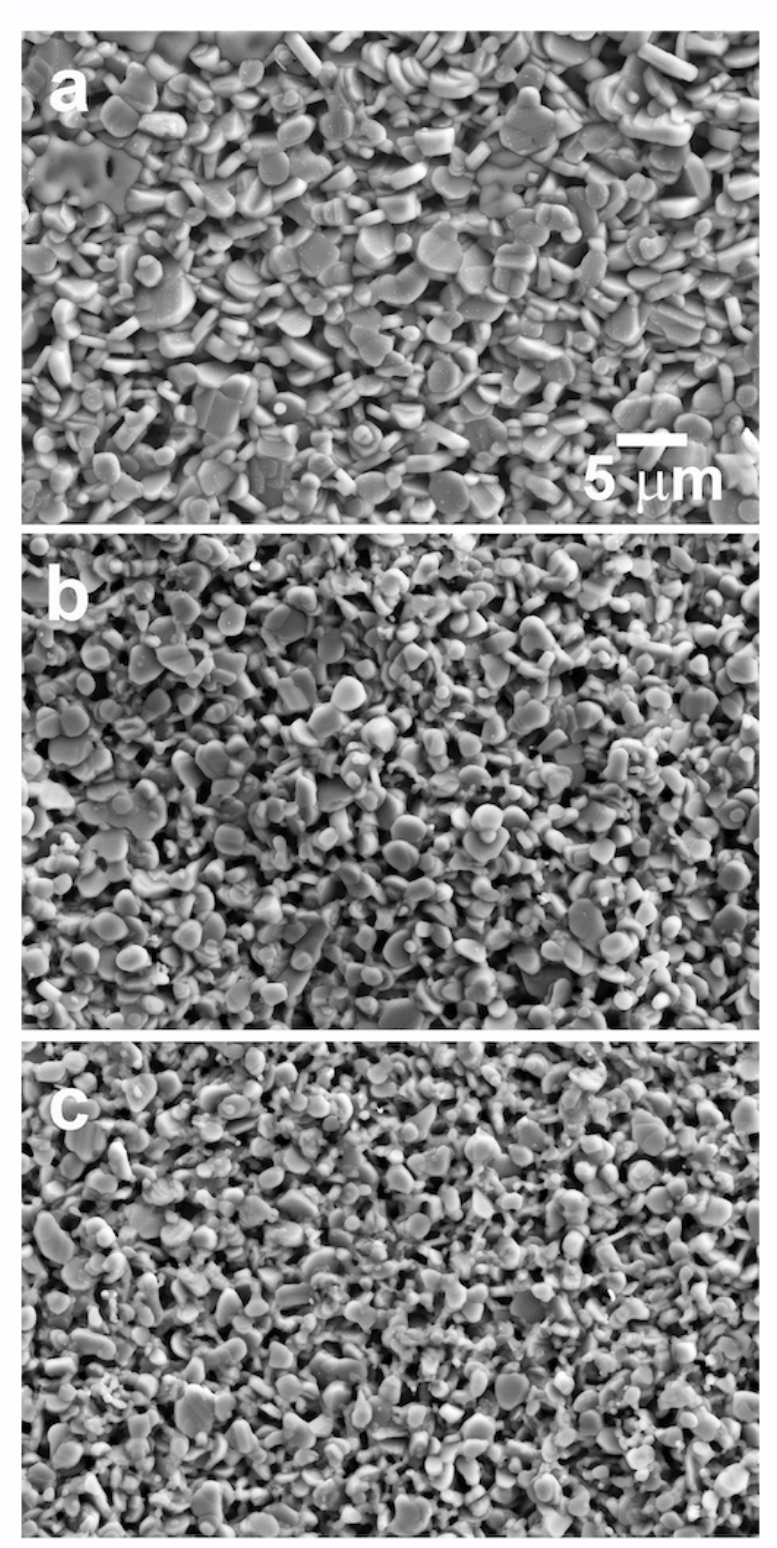

Figure 2

Representative SEM micrographs obtained on the surfaces of Ca3Co4O9 + x wt.% B4C samples, for x = 0.00 (a); 0.25 (b); and 0.75 (c).

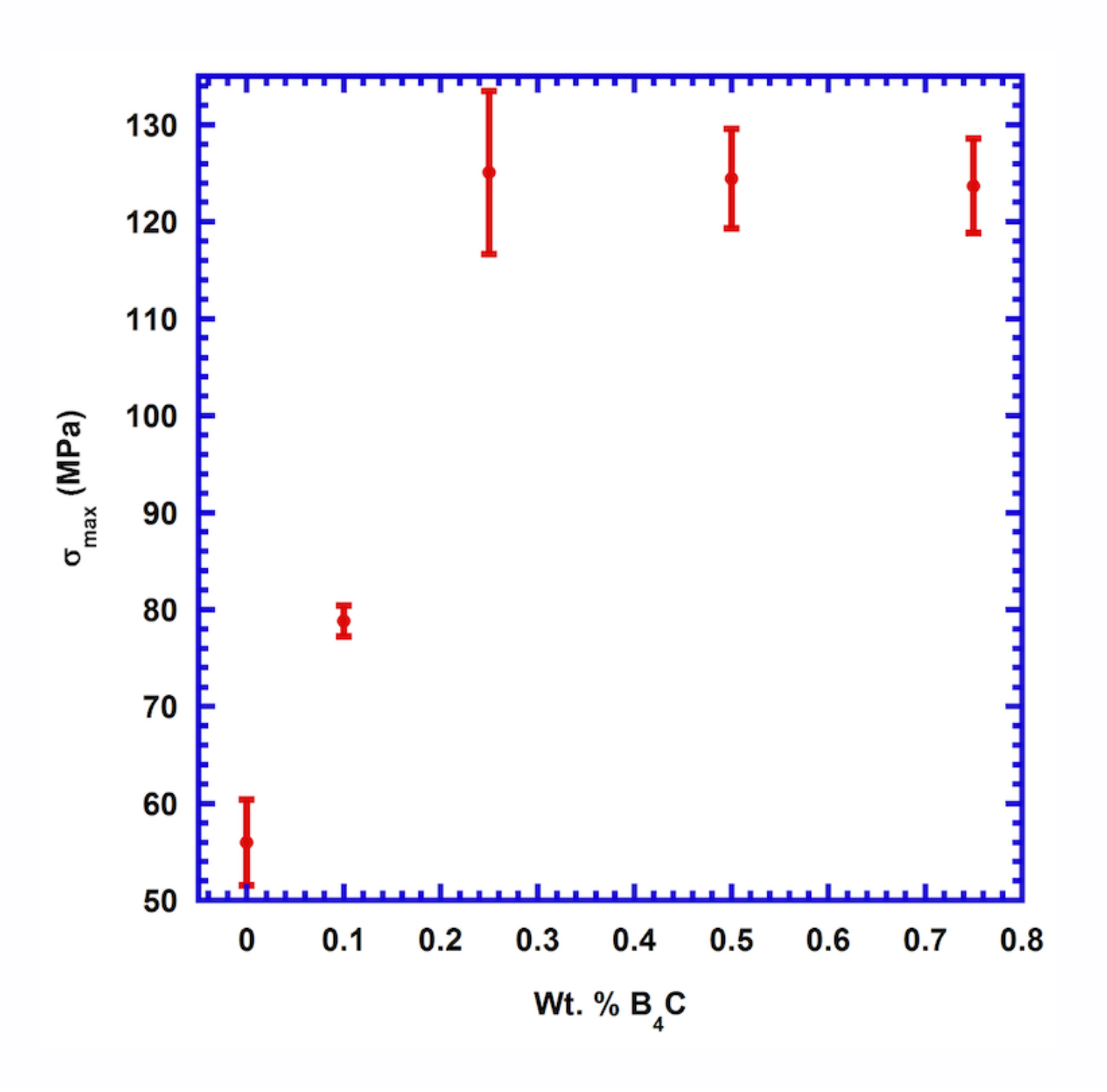

Figure 3

σmax values obtained through three point bending tests, with their standard error, as a function of B4C content.

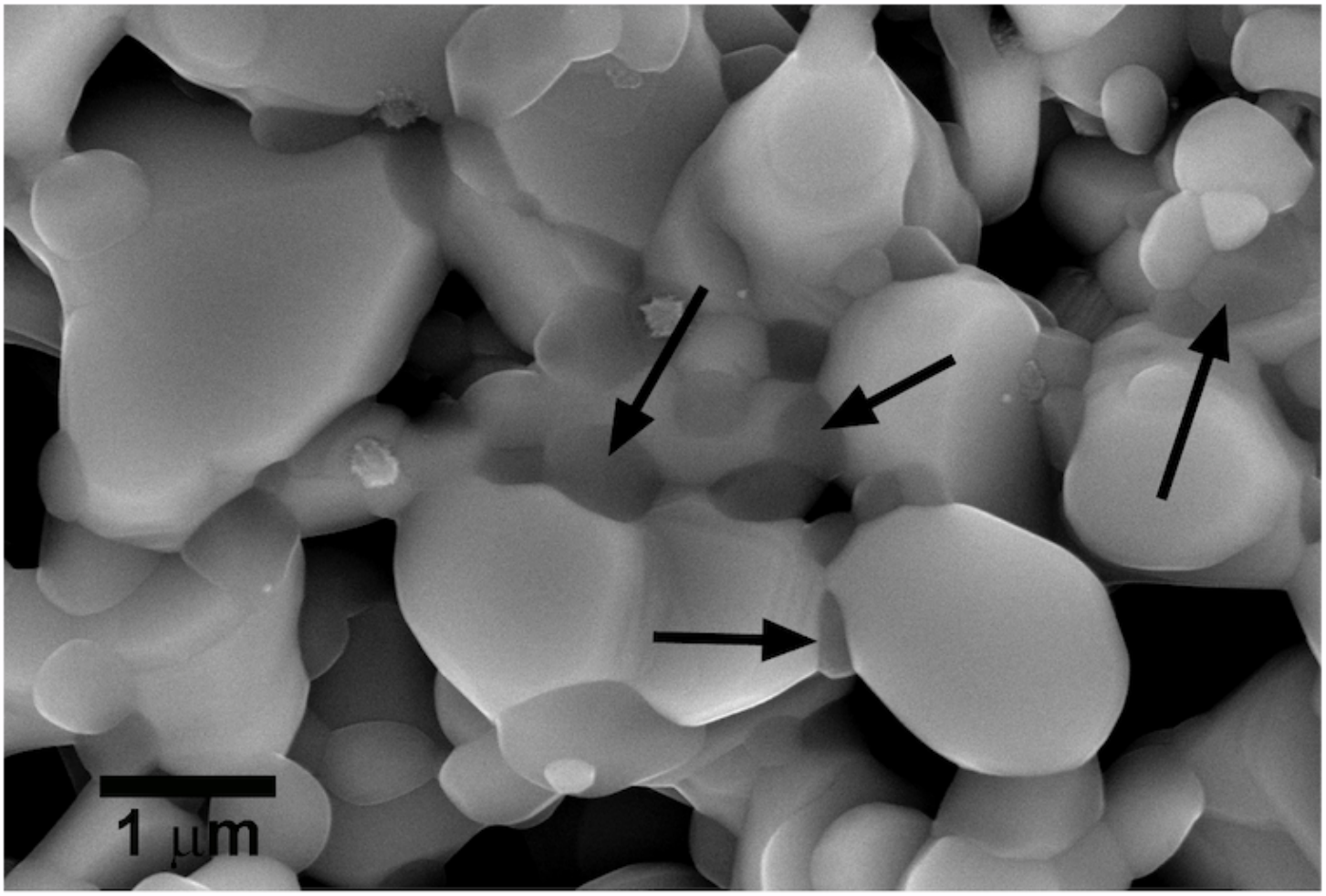

Figure 4

Representative SEM micrograph obtained in a fractured surface of Ca3Co4O9 + 0.75 wt.% B4C. The arrows show the dark grey contrast which corresponds to a B-rich phase.

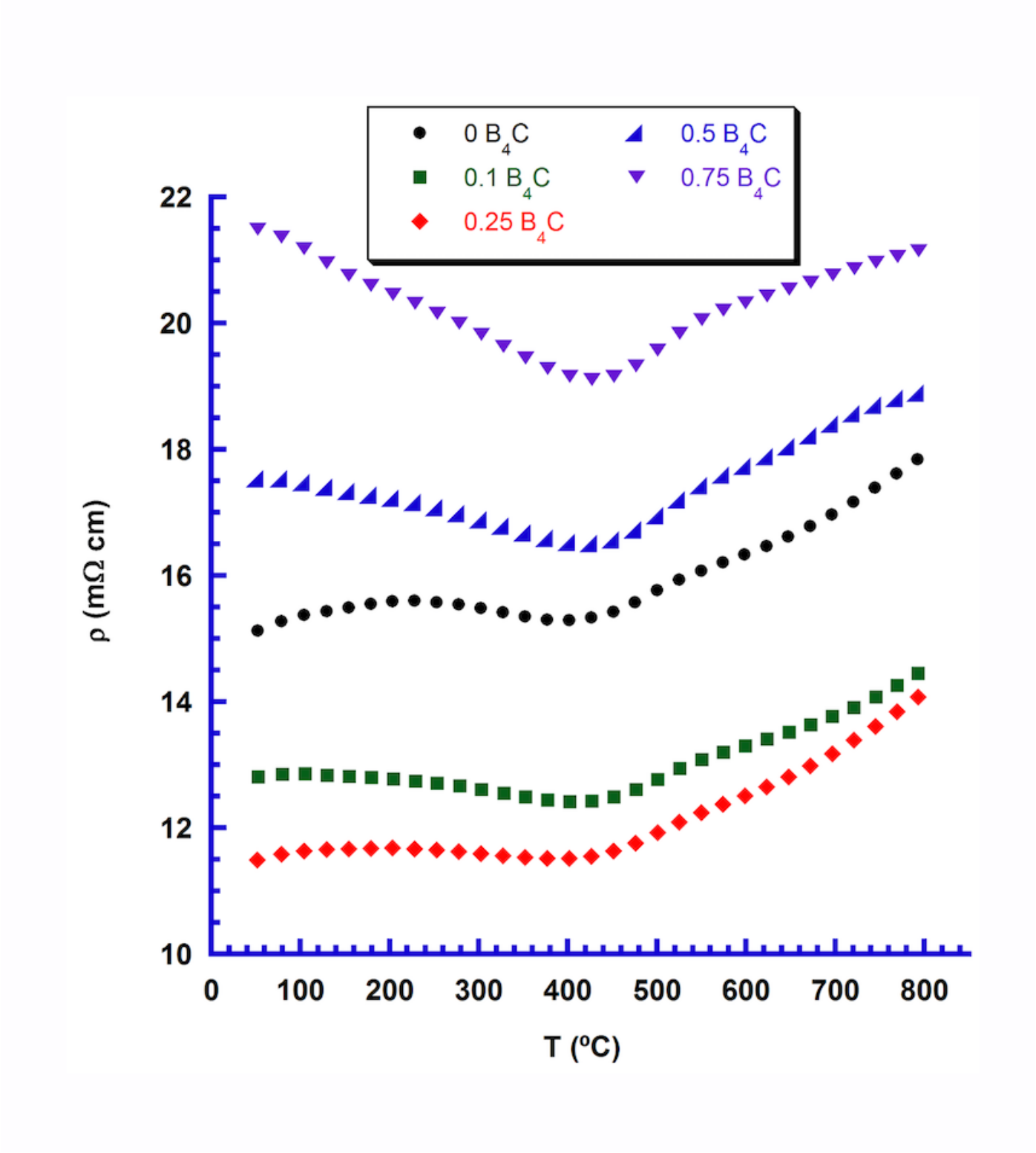

Figure 5

Electrical resistivity variation with temperature, as a function of B4C content, in Ca3Co4O9 + x wt.% B4C samples.

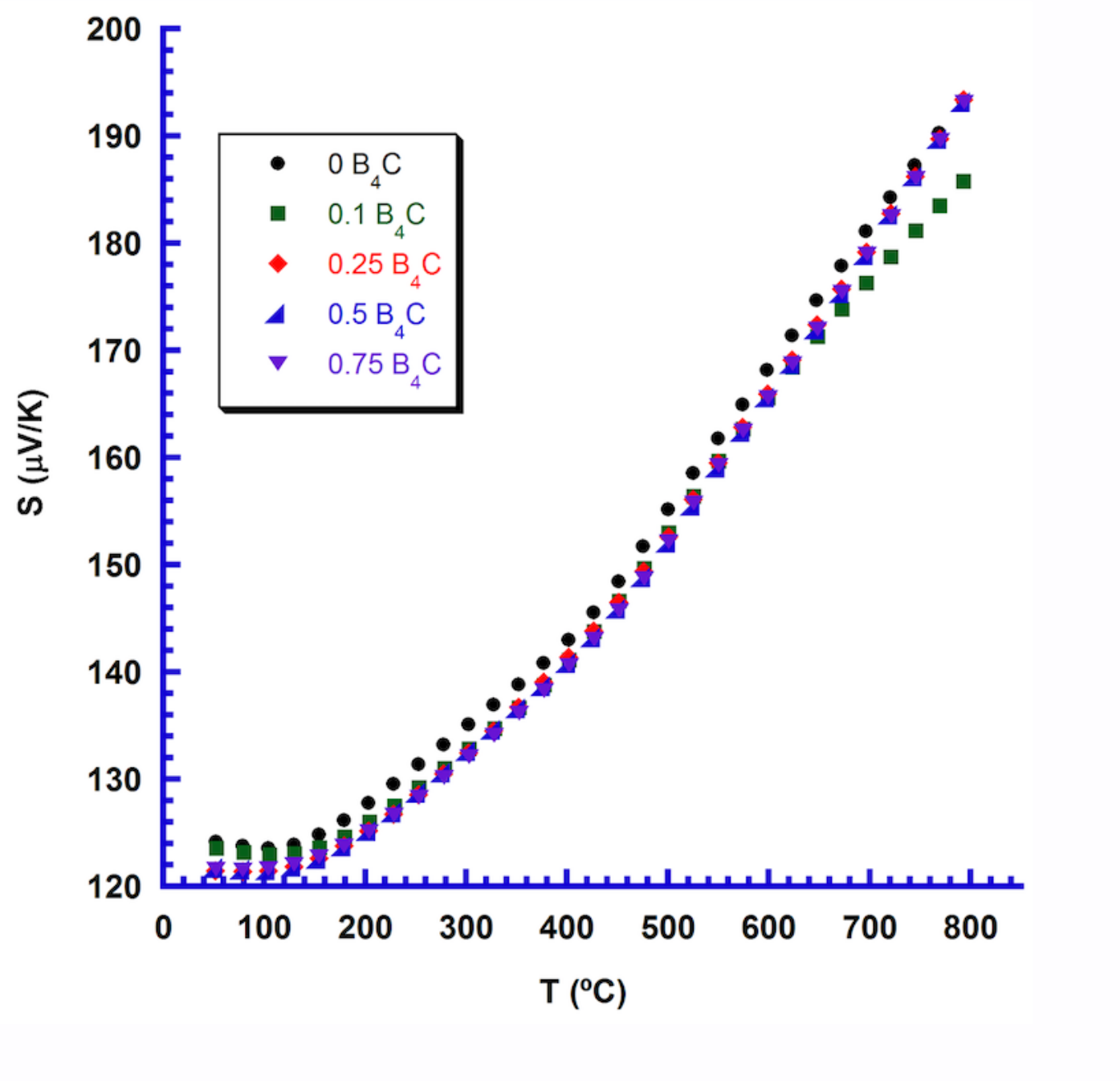

Figure 6

Seebeck coefficient variation with temperature, as a function of B4C content, in Ca3Co4O9 + x wt.% B4C samples.

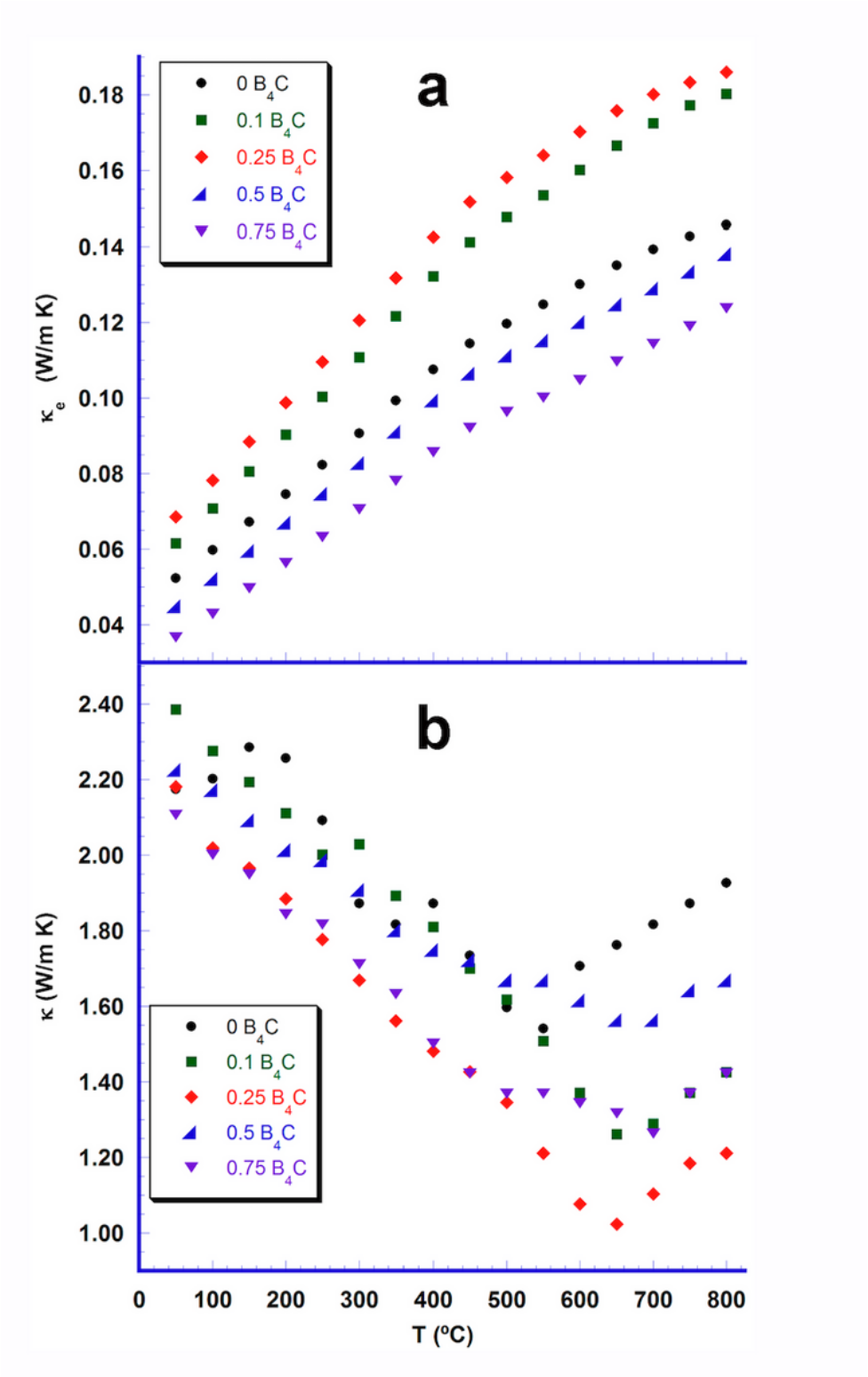

Figure 7

Evolution of a) Electronic thermal conductivity; and b) Total thermal conductivity, with temperature, as a function of B4C content, in Ca3Co4O9 + x wt.% B4C samples.

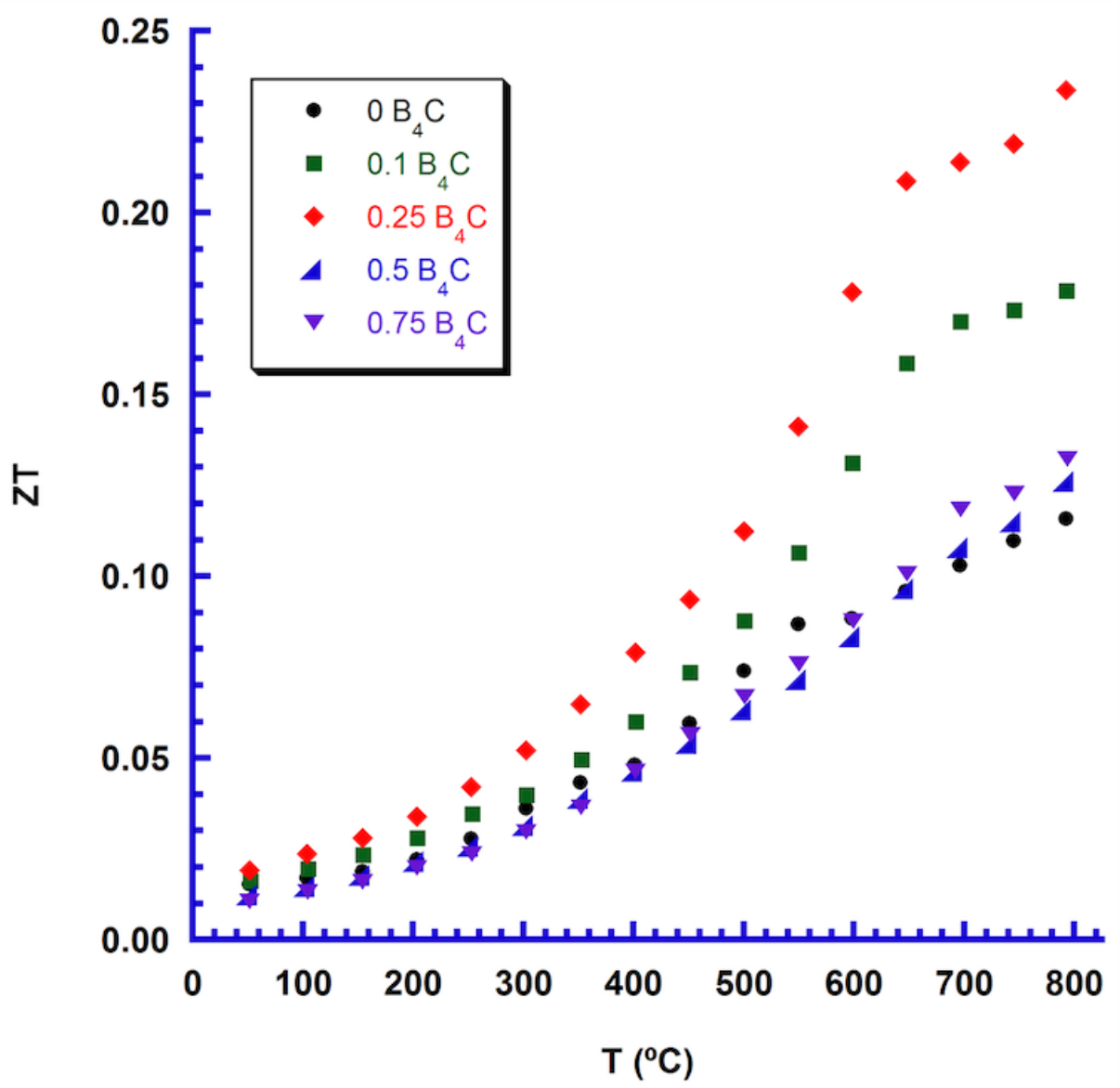

Figure 8

ZT evolution with temperature, as a function of B4C addition in Ca3Co4O9 + x wt.% B4C samples.